Production of spherical Inconel 625 powder for additive manufacturing by plasma-arc wire atomization: Influence of non-transferred and transferred arc modes on fine powder yield

Volodymyr Korzhyk[1,2], Dmytro Strohonov[2], Shiyi Gao[1*], Oleksii Tereshchenko[2], Oleksii Demianov[2], Oleg Ganushchak[2], Xinxin Wang[1]

[1] China-Ukraine Institute of Welding, Guangdong Academy of Sciences, Guangdong Provincial Key Laboratory of Material Joining and Advanced Manufacturing: 363, Changxing Road, Tianhe, Guangzhou, 510650, China
[2] E.O. Paton Electric Welding Institute (PEWI), National Academy of Sciences of Ukraine, 11 Kazymyr Malevych St., 03150 Kyiv, Ukraine
* Corresponding author's e-mail: meshiyigao@163.com

ABSTRACT

The possibility of producing spherical powder from Inconel 625 nickel-based superalloy using plasma-arc wire atomization technology in both non-transferred and transferred arc modes has been experimentally confirmed. Particle size distribution analysis showed that using the non-transferred arc mode reduces the average powder diameter by 23% compared to the transferred arc mode and increases the yield of the fine fraction (below 63 µm) from 40 to 62 wt.%. This increase in powder dispersity is achieved by using a reverse-polarity plasma torch with a hollow copper electrode and a divergent plasma-forming nozzle, which enables the formation of a high-velocity plasma jet. Morphological analysis showed that the powder has a regular spherical shape, with a sphericity coefficient close to 0.9. The powder microstructure is characterized by the absence of internal pores, which are typically found in gas atomized powders. Chemical composition analysis using energy-dispersive X-ray spectroscopy confirmed full compliance of the powder with the original feedstock wire material. Based on these results, plasma-arc wire atomization is recommended as an effective method for producing spherical Inconel 625 powder, fully meeting the requirements for fine powders in additive manufacturing applications.

Keywords: plasma-arc wire atomization, nickel-based alloy, spherical powder, particle size distribution, additive manufacturing.

INTRODUCTION

There is a growing demand for the repair and production of complex geometry parts from nickel-based superalloys using metal powder-based additive manufacturing (AM) processes [1–10]. The first group of powder-based AM processes, known as powder bed fusion (PBF), includes methods such as selective laser melting (SLM), direct metal laser sintering (DMLS), selective laser sintering (SLS) and electron beam melting (EBM). Another major group comprises direct energy deposition (DED) methods, including laser direct energy deposition process (LDED), plasma metal deposition (PMD), and cold spraying (CS). All of these AM processes employ spherical powders as feedstock materials for layer-by-layer deposition. These powders must meet stringent specifications in terms of particle size distribution, morphology, as well as physicochemical and technological properties. Particularly, SLM and CS processes require fine powders with a narrow size range of 15–45 µm, EBM utilizes 45–106 µm powders, LDED requires 45–150 µm, while PMD technology operates with powders ranging 63–160 µm [6–10]. In addition, these powders should exhibit a highly spherical shape with minimal external (satellites) and internal (pores) defects, superior

technological properties (e.g., high flowability, apparent density, sphericity coefficient), and a low gas content. These characteristics ensure high packing density of the deposited layers, reduced porosity, and improved mechanical properties of the final products [4, 5].

Various methods are employed to produce spherical metal powders for AM. These include various gas atomization (GA) methods [7, 10], the plasma rotating electrode process (PREP) [11], and plasma atomization (PA) of wire materials [12, 13]. Among them, GA is the most widely adopted method for producing spherical nickel-based alloys powders. GA processes mainly include vacuum induction melting inert gas atomization (VIGA) and electrode induction melting inert gas atomization (EIGA) techniques [7, 14, 15]. The main advantage of GA methods is their high productivity, which can reach 20–80 kg/h. Experimental studies on the particle size distribution of Inconel 718 nickel-based alloy powder produced via VIGA have shown that by adjusting the atomizing gas pressure within the range of 50–60 bar, and using a nozzle designed to generate a supersonic cold gas jet, powders with a size distribution of up to 150 μm can be obtained. The average particle diameter is d_{50} = 60–80 μm, while the fine fraction of powder (-63 μm) can constitute up to 40 wt.% [14]. However [16, 17], GA methods also have limitations, notably the formation of particles with gas-entrapped closed pores. These defects occur due to entrapment of gas by molten droplets followed by rapid solidification. For instance, Inconel 625 powder produced via GA can exhibit porosity levels of up to 3 vol.% [18]. Additionally, the porosity volume in powders produced by GA is generally higher compared to powders obtained using other methods, such as PREP and PA [9]. The presence of pores in powders can lead to the formation of defects in deposited layers, ultimately degrading the mechanical properties of the final product [19–20]. Another drawback of GA methods is the formation of satellite particles, primarily in the recirculation zone at the gas jet nozzle exit, along with irregularly shaped particles due to interactions between molten droplets and the cold gas jet [15, 21]. These defects increase particle adhesion and internal friction within the powder due to greater irregularity and increased interparticle contact surface area. As a consequence, the technological properties and packing characteristics of the powder, particularly its flowability and apparent density, are significantly reduced [22, 23]. Impairment of powder flowability during AM process

leads to uneven layer formation and decreased process stability. This can negatively impact the quality of metal AM parts, contributing to defects such as voids and microcracks, which in turn reduce the mechanical properties of the final part at both room and elevated temperatures [6, 8].

Thus, the formation of pores, satellites, and irregularly shaped particles in GA powders remains a critical unresolved issue, limiting their application in AM processes. Other commercially available method for producing spherical powder is PREP [24]. This method is based on melting and partial atomization of the rotating electrode's end face using a plasma jet. The existing equipment enables adjustment of the workpiece rotation speed from 20,000 to 40,000 rpm [25], thereby allowing control over powder size, as atomization occurs primarily due to centrifugal forces [26, 27]. Such an atomization scheme minimizes the aerodynamic impact of the plasma jet on the powder shape formation process. As a result, PREP powders exhibit near-perfect sphericity (sphericity coefficient 0.94–0.99), superior flowability and bulk density, and a complete absence of satellites, pores, and irregularly shaped particles commonly found in GA powders [22, 28]. Experimental studies on the application of Inconel 718 powder produced via PREP in SLM and EBM processes have shown that AM parts manufactured using PREP powder demonstrate a finer microstructure, lower chemical element segregation, and improved mechanical properties [29, 30]. However, despite these advantages, PREP process has several significant equipment-related limitations, primarily due to the difficulty of producing powder below 106 μm and the challenges associated with manufacturing of electrode rod feedstock with high surface quality [31].

A substantial increase in the electrode rotation speed (above 30,000 rpm) is required to obtain a yield of powder smaller than 106 μm exceeding 40 wt.% [11, 31]. This, in turn, complicates the already intricate kinematic scheme of the PREP unit, necessitating vibration reduction measures, advanced bearing system designs, and other technical solutions. Moreover, challenges arise in manufacturing cylindrical feedstock with precise dimensions, which must be ground with high accuracy [31]. In this context, promising alternatives for producing spherical powders involve technologies that use wire or rod feedstock, where the heating, melting, and atomization processes are carried out by plasma jets without the need for centrifugal forces

or high-speed rotational equipment with complex kinematic systems [32–34]. These technologies include plasma-arc wire atomization (PA) process in two variations: non-transferred and transferred arc modes. Studies [32, 35] have shown that the non-transferred PA process enables the production of high-quality Inconel 718 and Ti-6Al-4V alloy powder, with a sphericity coefficient of 0.94–0.97 and an average particle diameter $d_{50} = 60–75$ µm. The yield of defective particles does not exceed 1 wt.%, making the powder properties comparable to those of powder produced by the PREP method. The authors [32] have demonstrated that the use of a supersonic plasma system with three plasma torches enables the production of ultra-fine spherical Ti-6Al-4V alloy powder with an average particle diameter $d_{50} = 15–30$ µm, where nearly 100 wt.% is suitable for SLM/SLS applications. However, a significant drawback of PA process in its non-transferred arc mode is its low productivity, which does not exceed 1 kg/h [32].

An alternative approach to improving the efficiency of PA involves the use of the transferred arc scheme [35, 36]. By transferring the anode potential of the plasma arc from the plasma torch nozzle to the atomized wire, the heat input into wire is significantly increased due to the transition from convective heating to electron bombardment in the anode spot. In this case, the process productivity can be increased to 8–12 kg/h. Nevertheless, PA methods are still in the early stages of development and are only beginning to find practical application in the production of spherical powders for AM. This underscores the need for further in-depth research, particularly in the production of powders from Inconel 625 and Inconel 718 alloys, which are widely used in the aerospace, space, energy, and chemical industries. Currently, there is a lack of experimental data confirming the feasibility and economic viability of using PA methods for producing spherical powders from nickel-based alloys. Therefore, the objective of this study is to analyze the feasibility and assess the prospects of applying PA technology, in both non-transferred and transferred arc modes, for the production of spherical powders

from Inconel 625 alloy. To achieve this objective, the following tasks are set:

- investigate the particle size distribution, morphology, technological properties, and chemical composition of Inconel 625 powder produced by PA technology, in both non-transferred and transferred arc modes using plasma torches with copper hollow electrodes;
- perform a comparative analysis of the technological properties of the powder and the techno-economic characteristics of the aforementioned methods;
- provide recommendations for the potential practical application of the produced powders.

To address these objectives, a series of experimental studies was conducted using plasma-arc wire atomization in both non-transferred and transferred arc modes. The materials, setup, and methods used in this study are described below.

MATERIAL AND METHODS

Material for atomization

A solid wire made of Inconel 625 nickel-based alloy with a diameter of 1.2 mm was used as the atomized material (Table 1).

Wire atomization methodology

The experiments were conducted using plasma-arc equipment manufactured by LLC Scientific and Production Center 'Plazer', Ukraine:
1. PA in non-transferred arc mode, using the Plazer 180 PL-S system.
2. PA in transferred arc mode, using the Plazer 50 PL-W system.

For the PA process, experimental plasma torches with copper hollow electrodes were used, operating at reverse polarity (RPT) (Figures 1, 2).

In general, the PA process involves melting and dispersing a consumable wire that is fed into the high-velocity plasma jet zone (Figure 1a, Figure 2a). In the non-transferred arc mode, the plasma arc forms between a hollow copper electrode

Table 1. Chemical composition of Inconel 625 solid wire

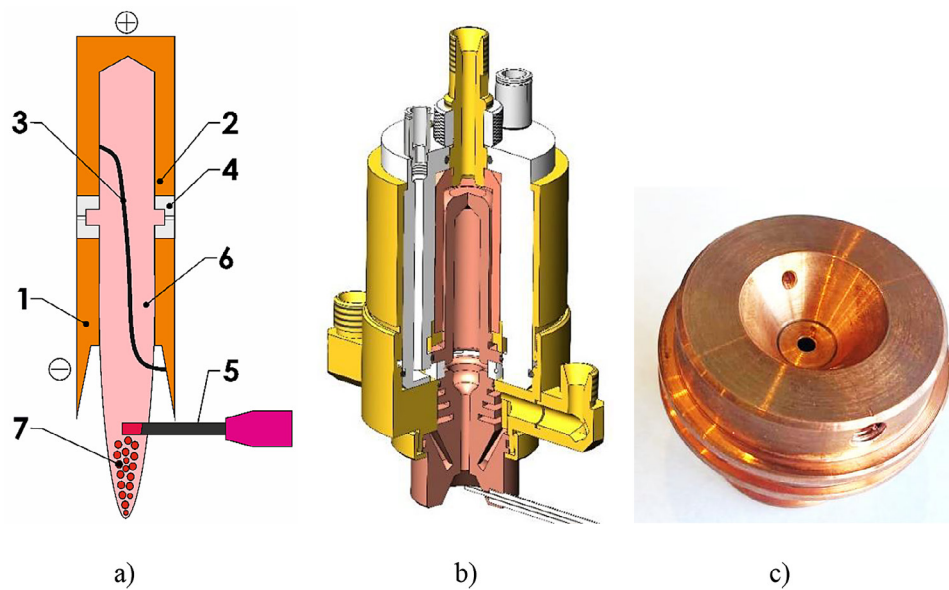| Chemical composition, wt. %												
Ni	Cr	Mo	Fe	Nb+Ta	Co	Si	Mn	Ti	Al	C	S	P
bal.	22	9	<5	3.5	<1	<0.5	<0.5	<0.4	<0.4	<0.1	<0.015	<0.015

Figure 1. Atomization scheme (a), 3D model of a plasma torch (b), and photograph (c) of the plasma-forming nozzle used in PA-RPT process in non-transferred arc mode, where: 1 – plasma-forming divergent nozzle (cathode); 2 – hollow copper electrode (anode); 3 – plasma arc; 4 – swirl-ring; 5 – atomized wire; 6 – high-velocity plasma jet; 7 – powder
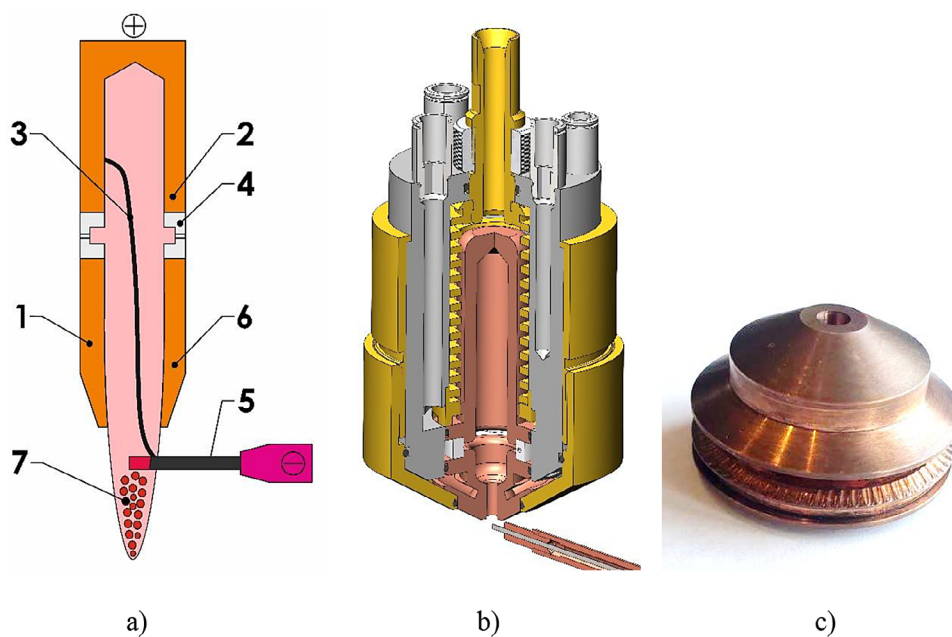

Figure 2. Atomization scheme (a), 3D model of a plasma torch (b), and photograph (c) of the plasma-forming nozzle used in the PA-RPT process in transferred arc mode, where: 1 – plasma-forming nozzle; 2 – hollow copper electrode (anode); 3 – plasma arc; 4 – swirl-ring; 5 – atomized wire (cathode); 6 – high-velocity plasma jet; 7 – powder

(anode) and the plasma-forming nozzle (cathode), whereas in the transferred arc mode, it forms between the hollow copper electrode (anode) and the atomized wire (cathode) [36, 37]. Optimization of the technological parameters of PA-RPT process was carried out based on the results of

mathematical modeling and previous experimental studies [38–42]. The technological parameters of the PA-RPT process in transferred arc mode were as follows: arc current - 220 A; arc operating voltage – 190…200 V; plasma-forming gas (argon) flow rate - 250 l/min; wire feed rate - 13.4 m/min;

distance between the cathode and anode 8 mm. The parameters for the PA-RPT process in non-transferred arc mode were: arc current 300 A; arc operating voltage 135–140 V; plasma-forming gas (argon) flow rate 250 l/min; wire feed rate 2.9 m/min; distance from the plasma torch nozzle to the atomized wire 4 mm. Wire atomization was conducted in a laboratory-scale atomization chamber (Figure 3) under an argon atmosphere. To ensure an inert atmosphere, the atomization chamber was first evacuated to a residual pressure of $(5–7) \times 10^{-3}$ Torr before argon was introduced.
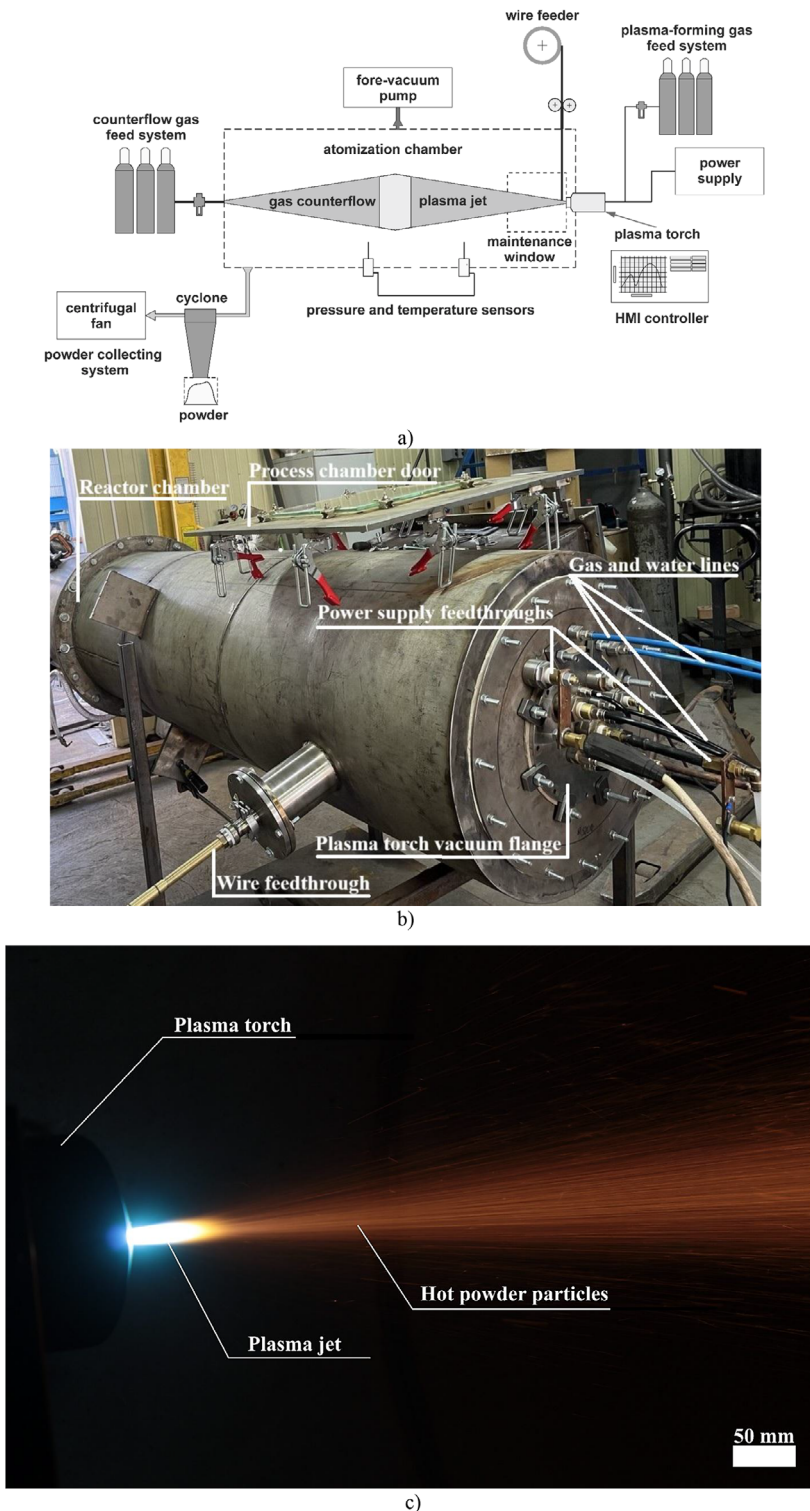

Figure 3. Schematic representation (a) and photograph (b) of the wire atomization chamber, along with visualization (c) of the PA-RPT process in transferred arc mode

Research methodology

Sieve analysis of the metal powder to determine its particle size distribution was performed in accordance with ASTM B214-22 standard using an AS-200U (Ukraine) impact sieve analyzer equipped with a set of sieves with aperture sizes ranging from 25 to 250 µm.

The morphology of the atomized powder was investigated using Scanning Electron Microscopy (SEM), images obtained with a VEGA 3 SBH EasyProbe (TESCAN, Czech Republic) equipped with a thermionic electron gun. The images were analyzed using MIPAR software (USA), following the methodology described in [43–52]. Loose powder samples were mounted on standard stubs using carbon adhesive tape.

The microstructure of the atomized powder was examined via metallographic analysis using a Neophot-32 (Carl Zeiss Jena, Germany) inverted metallographic microscope with a digital camera. Samples preparation included cutting with a IsoMet 1000 (Beuhler, USA) machine and diamond cut-off blades (diamond cut-off blade 11-4808E), embedding in resin, grinding with SiC waterproof abrasive papers (P400, P600 grit), and polishing using elastic diamond discs (A28/14 and A14/10), followed by a final polish with DiaDuo diamond suspension (3 µm) on a wool cloth.

The phase composition of the powder was analyzed by X-ray diffraction (XRD) using a DRON-M1 (Ukraine) X-ray diffractometer in monochromatized CuKα radiation. A graphite single crystal was used as a monochromator on the diffracted beam. Scanning was performed in Bragg-Brentano (2Θ) geometry over the range of 20° to 100°, with a step size of 0.03°, and an exposure time of 4 s. Diffractometric data were processed using the PowderCell 2.4 (Germany) software for full-profile analysis of X-ray spectra of the polycrystalline phase mixture.

A VEGA3 SBH EasyProbe SEM was also used for chemical composition analysis via Electron Probe Micro Analysis (EPMA) using a Quantax spectrometer (Bruker, Germany) with a XFlash 6-10 Energy-Dispersive X-ray Spectrometry (EDS) detector. The oxygen and nitrogen content in the atomized powders were measured using a TC-436 nitrogen/oxygen analyzer (LECO, USA).

Powder flowability was determined using a Hall flowmeter according to ASTM B213-20 standard, and the apparent density was measured in accordance with ASTM B212-21 standard.

Techno-economic analysis

The productivity of the PA-RPT process (G_a) was determined by the mass of powder (kg/h) collected from the atomization chamber over a period of one hour. The electrical power of the plasma torch (kW), recorded using the ammeter and voltmeter of the plasma torch power supply during the PA-RPT process, was calculated using the following equation:

$$P = I \cdot U \qquad (1)$$

where: I is the arc current (A), and U is the arc voltage (V).

The specific energy consumption (E_c) was calculated using the following equation:

$$E_c = \frac{P}{G_a} \qquad (2)$$

where: G_a is the productivity of the plasma sputtering process (kg/h), and P is the electrical power of the DC plasma torch (kW).

The specific gas consumption (G_c) was calculated using the following equation:

$$G_c = \frac{Q}{G_a} \qquad (3)$$

where: G_a is the productivity of the plasma sputtering process (kg/h), and Q is the plasma-forming gas flow rate (m³/h).

RESULTS

Figure 4 presents the results of the particle size distribution analysis of the atomized powders, showing that the PA-RPT process in non-transferred arc mode yields the highest proportion of fine powder. In this case, the primary powder fraction is less than 200 µm, with the fine fraction below 63 µm comprising up to 62 wt.%. For the transferred arc mode, the dominant fraction is less than 250 µm, while the fine fraction below 63 µm does not exceed 38 wt.%. Furthermore, the average particle diameter (d_{50}) for the non-transferred arc mode is 59 µm, compared to 77 µm for the transferred arc mode. Figure 5 illustrates the morphology of Inconel 625 powder (25–63 µm), produced via PA-RPT, in both non-transferred and transferred arc modes. The images
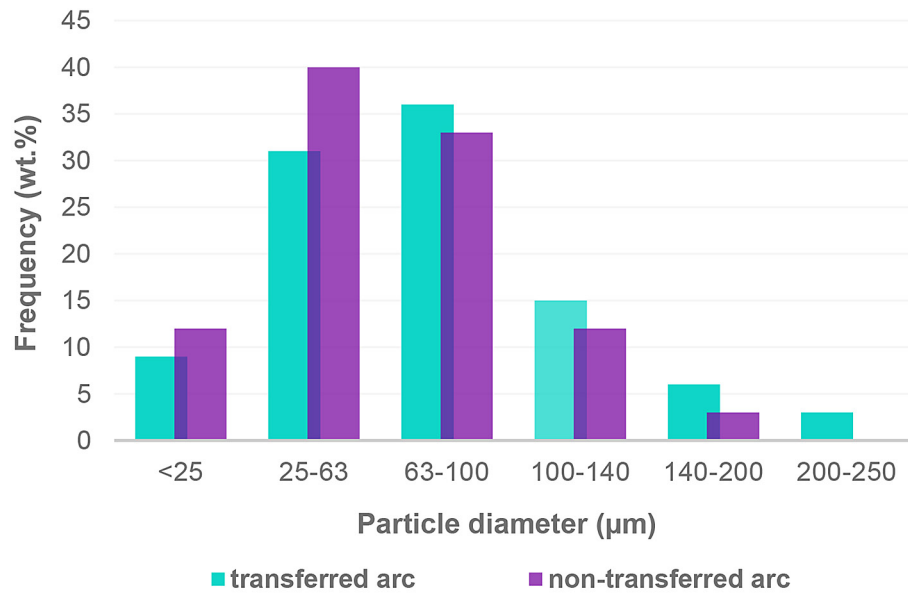
Figure 4. Particle size distribution of Inconel 625 powder produced via PA-RPT
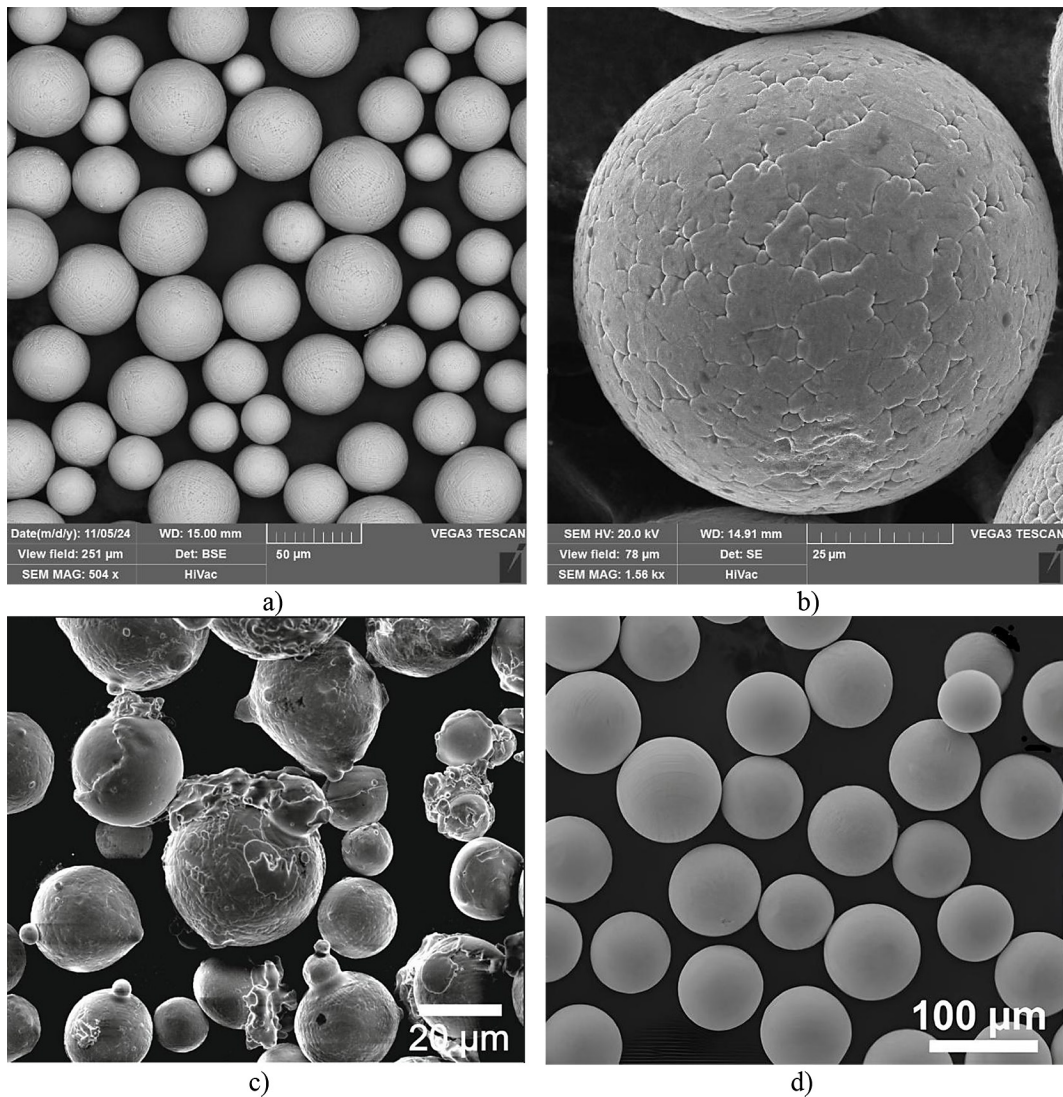

Figure 5. Morphology of Inconel 625 powder: (a, b) 25–63 µm produced via PA-RPT; (c) 15–45 µm produced via VIGA (Höganäs, Sweden) [53]; (d) Inconel 718 powder 45–106 µm, produced via PREP [54]
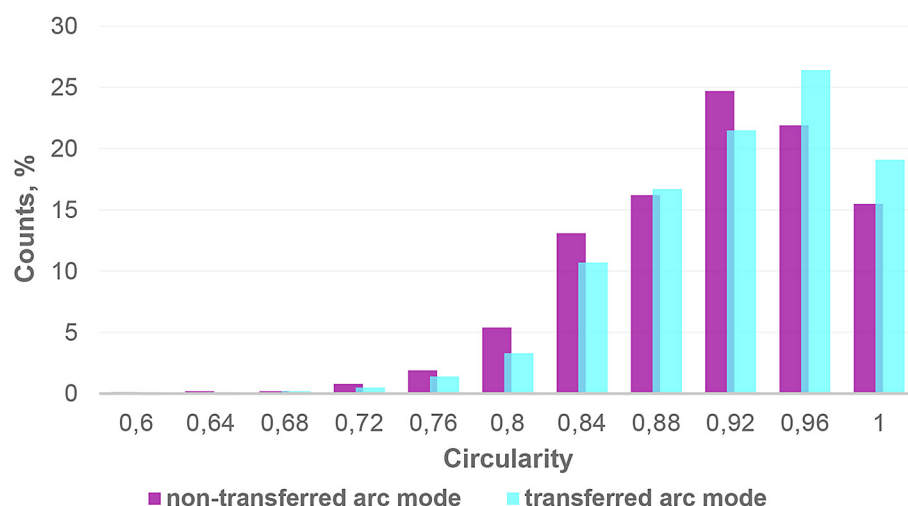
Figure 6. Circularity of Inconel 625 powder 25–63 µm produced by PA-RPT process

demonstrate that the powder exhibits a spherical shape, with no visible external defects such as cracks, satellites, open pores, or irregular particles. The proportion of such defects in the total powder batch does not exceed 1 wt.%. Analysis of MIPAR-processed images revealed that powders obtained via PA-RPT process exhibit highly spherical shape. For the transferred arc mode, the
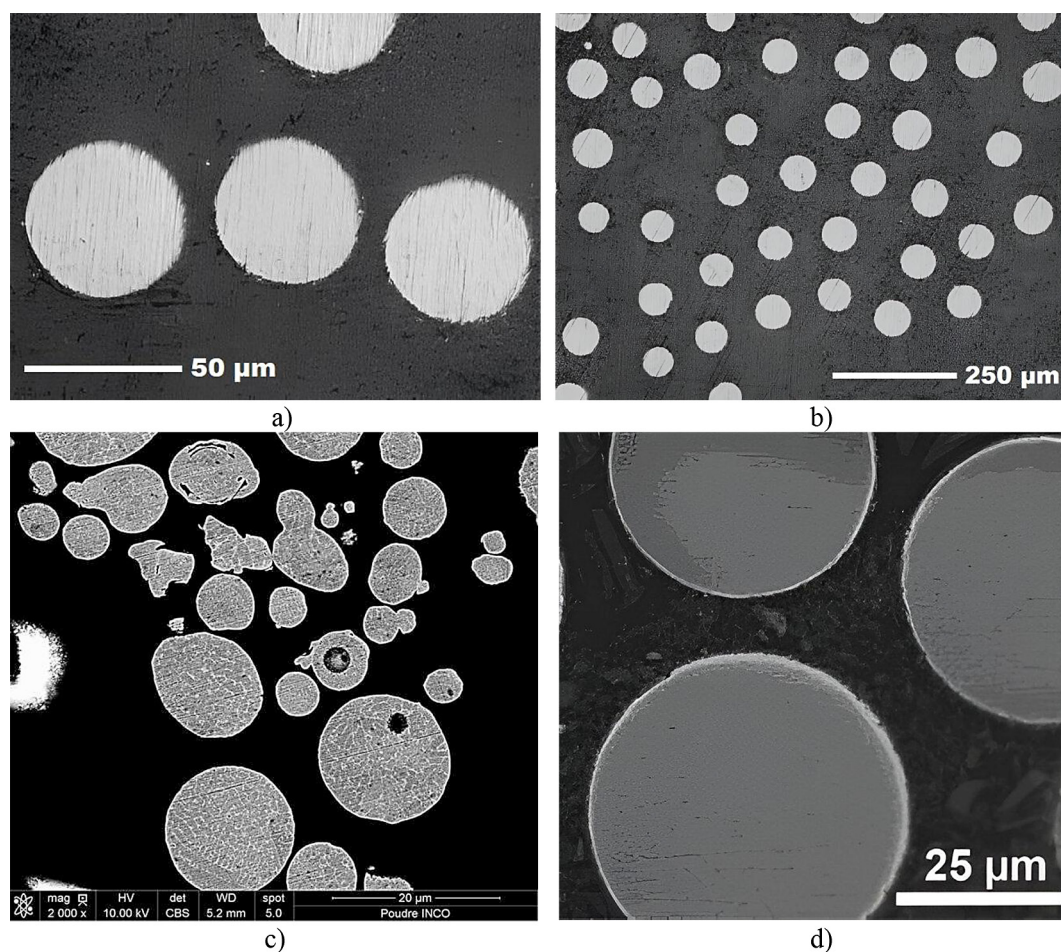

Figure 7. Cross-sectional images of Inconel 625 powder produced via PA-RPT: (a) 25–63 µm; (b) 63–106 µm; (c) Inconel 718 powder 5–25 µm, produced via VIGA [55]; (d) Inconel 718 powder 15–53 µm, produced via PREP [54]

average sphericity coefficient (circularity) is S = 0.89, whereas for the non-transferred arc mode it is S = 0.85 (Figure 6).

The analysis of the microstructure (Figure 7) of the Inconel 625 powder produced in both non-transferred and transferred arc modes reveals the absence of internal pores and voids.

According to the results of X-ray diffraction studies (Figure 8), it was established that the phase composition of the Inconel 625 powder in both non-transferred and transferred arc modes consists of a γ-phase solid solution of Ni-Cr with a face-centered cubic (FCC) lattice (Table 2). Using the EPMA method and the «TC-436 Nitrogen/Oxygen Analyzer» gas analyzer, the chemical composition of the Inconel 625 powder produced by the PA-RPT process in both non-transferred and transferred arc modes was determined (Table 3). Figure 9 shows the EDS elemental distribution across the surface of the Inconel 625 powder.

Table 4 presents the technological properties of both commercial and experimentally produced Inconel 625 powders, manufactured using GA-VIGA, PREP and PA-RPT methods.

The techno-economic analysis of the considered process revealed that the productivity of the PA process in non-transferred arc mode does not exceed 1.6 kg/h at a plasma torch power of 42 kW, whereas for transferred arc mode it reaches 7.4 kg/h at a power of 44 kW.

The specific energy consumption calculation (Figure 10) for producing 1 kg of Inconel 625 powder using PA-RPT process showed a value 26.3 kW/kg in non-transferred arc mode, compared to 5.9 kW/kg in transferred arc mode.

Gas to metal consumption calculation (Figure 11) for producing 1 kg of Inconel 625 powder using PA-RPT process showed a value 9.4 m^3/kg in non-transferred arc mode, compared to 2.0 m^3/kg in transferred arc mode.

DISCUSSION

Taking into account that the PA-RPT process in both non-transferred and transferred arc modes is carried out at nearly identical plasma jet power and gas flow rate – averaging 42–44 kW and 250 l/
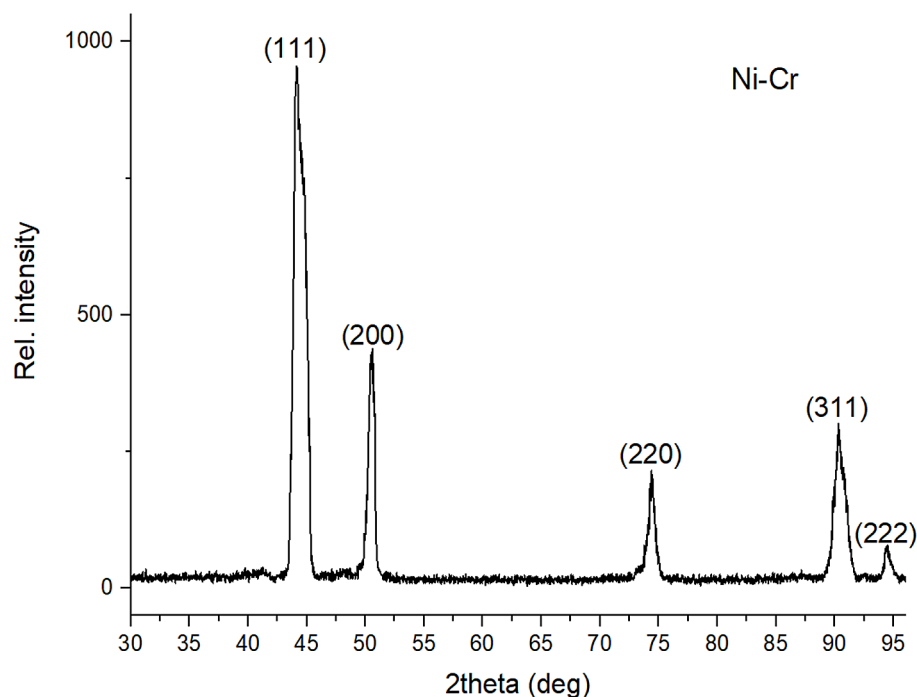

Figure 8. X-ray diffraction pattern of Inconel 625 powder 25–63 μm

Table 2. Results of XRD analysis of Inconel 625 powder produced via the PA-RPT process

№	Sample	Phases	Phase cont., % vol.	Lattice parameters, Å
1	Powder 25–63 μm	γ Ni-Cr	100	3.5991
2	Powder 45–106 μm			3.5997

Table 3. Chemical composition of Inconel 625 powder

Study area	Chemical composition, wt. %											
	Ni	Cr	Mo	Fe	Nb	Co	Si	Mn	Ti	Al	O	N
Wire	62.04	21.86	9.14	2.23	3.37	0.24	0.19	0.19	0.31	0.28	0.016	0.0035
Powder 25–63 µm	62.41	21.91	9.01	2.35	3.21	0.23	0.12	0.21	0.22	0.11	0.019	0.0038
Powder 45–106 µm	62.28	21.98	8.97	2.01	3.33	0.19	0.14	0.18	0.24	0.17	0.017	0.0034
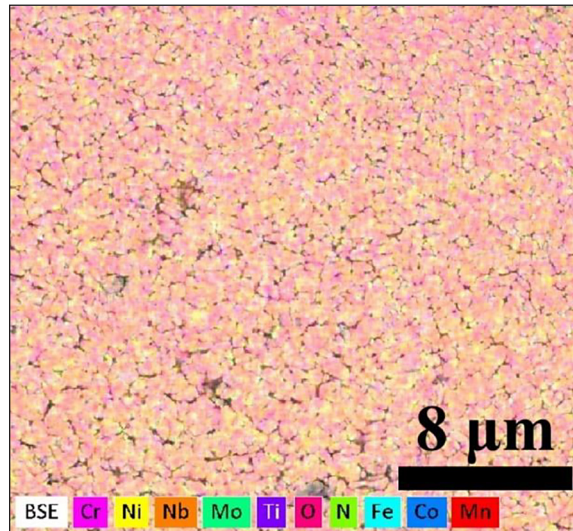
Figure 9. Results for EDS analysis for Inconel 625 powder

min, respectively – the significant increase by 63% in the yield of the fine fraction below 63 µm (Figure 4) observed in the non-transferred arc mode can be attributed to the higher gas-dynamic pressure exerted on the molten material of the wire tip. This effect is ensured by the design of the divergent plasma-forming nozzle and the specific nature of the PA-RPT process in the non-transferred mode, in which the compression and heating of the plasma jet primarily occur within the channel of the nozzle. As a result, the velocity of the plasma exiting the nozzle increases significantly and can reach supersonic levels – up to Mach 2 [32, 33]. Additionally, feeding the wire into the divergent conical section of the nozzle contributes to maintain both the velocity and gas-dynamic pressure of the plasma jet at the wire tip. In contrast, during the PA-RPT process in the transferred arc mode, the arc column primarily forms outside the plasma torch, beyond the nozzle channel, where the plasma flows freely into the open atmosphere. This PA atomization scheme and therefore the design of the plasma-forming nozzle - impedes effective arc compression, leading to a significant reduction in the gas-dynamic pressure of the plasma jet at the wire tip's melting zone. Consequently, larger primary droplets are formed, typically ranging in size from 600 to 800 microns [56]. Thus, the velocity of the plasma jet is a crucial parameter that allows for controlling the particle size in the PA process. Microstructural analysis (Figure 7) revealed that the Inconel 625 powder exhibits a complete absence of internal pores and voids, a feature not
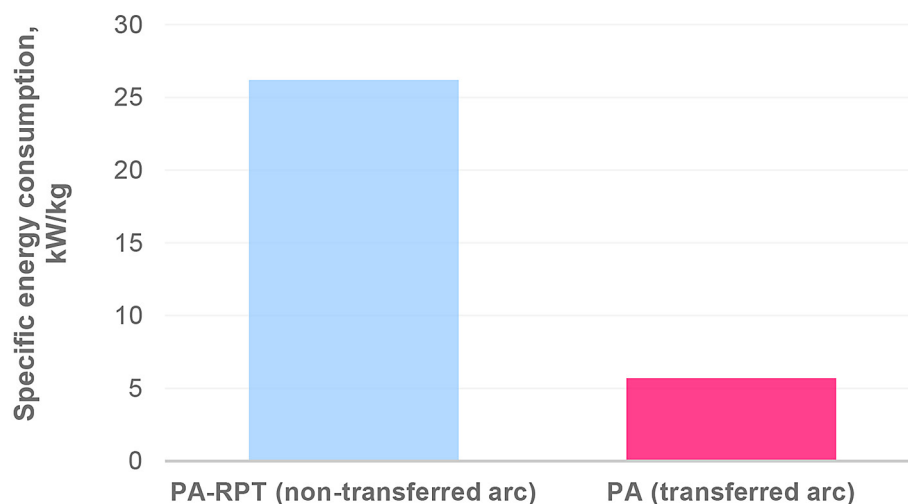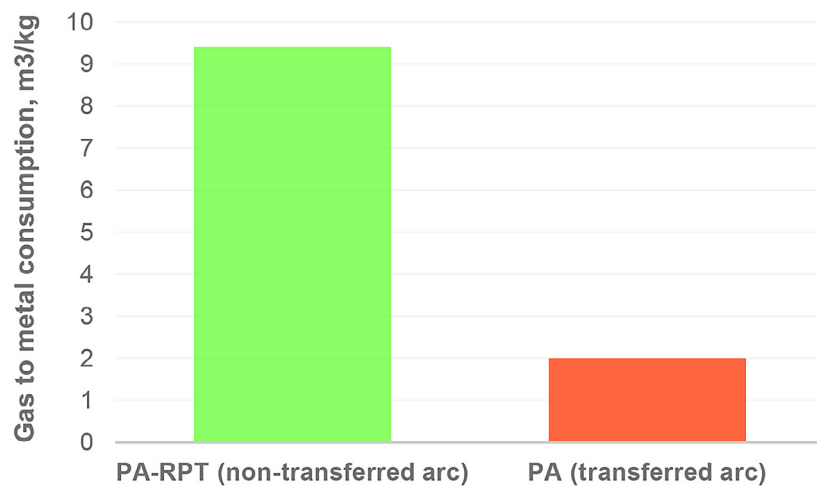

Figure 10. Specific energy consumption for producing 1 kg of Inconel 625 powder using PA-RPT process

Table 4. Technological properties of Inconel 625 powders produced by various atomization technologies

Method	Particle Size, µm *ASTM B214-22	Flowability, s/50g ASTM B213-20	Apparent density, g/cm³ ASTM B212-21
GA-VIGA (Höganäs, Sweden)	15–45	≤18	4.4
	45–106	≤15	4.6
	45–150	–	–
SS-PREP (Sino-euro Ltd, China)	15–45	12–15	4.8–5.0
	45–106		
	45–150		
PA-RPT non-transferred mode (PEWI, Ukraine)	*25–45	15.7	4.67
	*45–106	13.9	4.75
	*45–140	13.1	4.79
PA-RPT transferred arc mode (PEWI, Ukraine)	*25–45	15.8	4.70
	*45–106	13.4	4.79
	*45–140	12.3	4.84

Figure 11. Gas to metal consumption for producing 1 kg of Inconel 625 powder using PA-RPT process

typically observed in powders produced by GA methods. The observed differences in structural characteristics between powders manufactured by the PA-RPT process and GA techniques can be attributed to the following factors [15–17, 32]:

- The PA-RPT process involves significantly lower atomization pressures, typically not exceeding 4–10 bar. In contrast, GA methods operate at substantially higher pressures, ranging from 20 to 60 bar, which induces turbulent gas flow and promotes increased gas entrapment within the powder particles.
- Additionally, the PA-RPT process employs high-temperature gas at the plasma torch nozzle outlet, generally ranging from 4000 to 10,000 °C. This ensures extended residence time for molten particles in a 'hot' state, thereby enabling near-complete outgassing of any

entrapped gas. In contrast, GA methods employ cold gas jets for atomization, resulting in rapid solidification of the melt and consequently preventing sufficient degassing of the particle interiors.

XRD analysis showed that the phase composition of the Inconel 625 powder (Figure 8), produced by PA-RPT process in both non-transferred and transferred arc modes consists of a γ-phase solid solution of Ni-Cr with a FCC lattice (Table 2).

Chemical composition analysis of the feedstock wire and atomized Inconel 625 powder by EPMA-EDS (Table 3) confirmed that their chemical composition meets the requirements for the chemical composition of wires and rods from nickel-based alloys according to the ASTM B446-23 standard 'Standard specification for

Nickel-chromium-molybdenum-niobium alloy bars and billets'.

The EDS image (Figure 9) demonstrates that the chemical elements are uniformly distributed within the dendritic regions on the powder surface, indicating the absence of elemental segregation in the surface layer during the atomization and solidification processes.

The high sphericity values (Figures 5, 6) of the studied powders contribute to their superior technological properties (Table 3). These properties are comparable to those of powders produced using the Supreme Speed Plasma Rotating Electrode Process (SS-PREP) process, where the electrode rotation speed exceeds 30,000 rpm. Moreover, the technological characteristics of PA-RPT powder slightly surpass those of GA-VIGA powder in terms of flowability and apparent density. The superior technological properties of powders produced by the PA-RPT process, compared to GA powders, are primarily due to the absence of external defects such as satellites and the improved sphericity of the particles. These external imperfections and irregular shapes in GA powders contribute to higher particle adhesion and internal friction, owing to increased surface irregularity and contact area between particles. As a result, flowability and apparent density characteristics are slightly degraded [22, 23].

A techno-economic analysis of the PA-RPT process revealed that the transferred arc mode demonstrates approximately 4.5 times lower specific energy consumption per kilogram of produced powder (Figure 10), requiring only 5.9 kW/kg compared to 26.3 kW/kg in the non-transferred arc mode. This substantial difference is attributed to the distinct heating mechanism involved in the transferred arc mode. Unlike conventional heat exchange typical of the non-transferred arc mode, heat transfer in the transferred arc mode occurs primarily through electron bombardment. As electrons pass the arc column and decelerate in the anode region, they generate an excess negative charge that accumulates on the anode. This charge buildup significantly increases heat input into the atomized wire [56] and at the same plasma torch power boosts productivity by more than 4.6 times – reaching 7.4 kg. An increase in process productivity at constant plasma torch power leads to a 4.7 times reduction in gas consumption per kilogram of powder produced (Figure 11), amounting to 2.0 m³/kg in the transferred arc mode and 9.4 m³/kg in the non-transferred arc mode, respectively.

CONCLUSIONS

Inconel 625 powder produced by PA-RPT process, under both non-transferred and transferred arc modes demonstrates high surface quality and excellent sphericity, with no observable defects such as satellites, irregular shape particles, or internal porosity. Chemical composition analysis confirmed conformity with the elemental composition of the original wire feedstock material.

Experimental results confirmed that the PA-RPT process operating in non-transferred arc mode leads to a reduction in powder particle size compared to the transferred arc mode. Particularly, the average particle diameter (d_{50}) decreases by 23%, from 77 µm to 59 µm. Additionally, the yield of the fine fraction below 63 µm increases significantly, from 40 wt.% to 62 wt.% in the non-transferred arc mode.

A comparative techno-economic analysis of the PA-RPT process demonstrated that operation in transferred arc mode is significantly more cost-effective. It enhances process productivity by 4.6 times, achieving a production rate of 7.4 kg/h for Inconel 625 powder. Moreover, it reduces specific energy consumption by 4.5 times, reaching 5.9 kW/kg, and decreases gas consumption by 4.7 times, down to 2.0 m³/kg, compared to the non-transferred arc mode.

The obtained results indicate that the PA-RPT process is an effective technology for producing high-quality, spherical Inconel 625 powder, with technological characteristics comparable to those achieved by the industrial-scale SS-PREP process. Furthermore, powders produced by the PA-RPT process exhibit superior properties when compared to those manufactured via GA methods. The particle size distribution, chemical composition and technological properties of Inconel 625 powder, produced by PA-RPT makes it highly suitable for AM processes, particularly for EMB, LDED and PMD techniques.

REFERENCES

1. Zafar, F., Emadinia, O., Conceição, J. et al.: A Review on Direct Laser Deposition of Inconel 625 and Inconel 625-Based Composites - Challenges and Prospects. Metals. 2023; (13), 787 https://doi.org/10.3390/met13040787

2. Su, G., Shi, Y. Li, G. et al.: Improving the deposition efficiency and mechanical properties of additive manufactured Inconel 625 through hot wire laser metal deposition. Journal of Materials Processing Technology. 2023; (322), 118175. https://doi.org/10.1016/j.jmatprotec.2023.118175

3. Danielewski, H., Radek, N., Orman, L. et al.: Laser metal deposition of Inconel 625 Alloy – comparison of powder and filler wire methods. Materials Research Proceedings. 2023; (34), 154–160 https://doi.org/10.21741/9781644902691-19

4. Mao, D., Xie, Y., Meng, X. et al.: Strength-ductility materials by engineering a coherent interface at in coherent precipitates. Materials Horizons. 2024; (14), 3408–3419. https://doi.org/10.1039/D4MH00139G

5. Okuniewski, W., Walczak, M., Szala, M. et al.: Effect of surface modification by shot peening on cavitation erosion resistance of titanium alloy Ti-6Al-4V produced by DMLS method. Engineering Failure Analysis. 2025; (176), 109653. https://doi.org/10.1016/j.engfailanal.2025.109653

6. Swietlicki, A., Walczak, M., Szala, M.: Corrosion resistance of additive manufactured 17-4PH DMLS steel after heat treatment and shot peening process. Acta Mechanica et Automatica. 2025; (19), 205–211. https://doi.org/10.2478/ama-2025-0024

7. Hassila C., Paschalidou, M., Harlin, P. et al.: Potential of nitrogen atomized alloy 625 in the powder bed fusion laser beam process. Materials and Design 2022; (221), 110928. https://doi.org/10.1016/j.matdes.2022.110928

8. Rehman, A., Karakas, B., Mahmood, M. et al.: Additive manufacturing of Inconel-625: from powder production to bulk samples printing. Rapid Prototyping Journal 2023; 9(23), 1788–1799. https://doi.org/10.1108/RPJ-11-2022-0373

9. Chen, G., Zhao S., Tan P. et al.: A comparative study of Ti-6Al-4V powders for additive manufacturing by gas atomization, plasma rotating electrode process and plasma atomization. Powder Technology. 2018; (333), 38–46. https://doi.org/10.1016/j.powtec.2018.04.013

10. Sun, P., Fang, Z., Zhang, Y. et al.: Review of the methods for the production of spherical Ti and Ti alloy powder. JOM. 2017; (69), 1853–1860. https://doi.org/10.1007/s11837-017-2513-5

11. Fan, X., Tian, Q., Chu, X. et al.: Microstructure and mechanical properties of Co31.5Cr7Fe30Ni31.5 high-entropy alloy powder produced by plasma rotating electrode process and its applications in additive manufacturing. Journal of Materials Research and Technology. 2024; (31), 1924–1938. https://doi.org/10.1016/j.jmrt.2024.06.217

12. Yurtukan, E., Unal, R.: Theoretical and experimental investigation of Ti alloy powder production using low-power plasma torches. Transactions of Nonferrous Metals Society of China. 2022; (32), 175–191. https://doi.org/10.1016/S1003-6326(21)65786-2

13. Prokopov, V., Fialko, N., Sherenkovskaya, G. et al.: Effect of the coating porosity on the processes of heat transfer under, gas-thermal atomization. Powder Metall. Met. Ceram. 1993; (32), 118–121. https://doi.org/10.1007/BF00560034

14. Shang, F., Chen, S., Wei, M. et al.: The structure and properties of Inconel 718 superalloy powder prepared by vacuum induction melting gas atomization for laser direct metal deposition. Materials Research Express. 2019; (6), 026566. https://doi.org/10.1088/2053-1591/aaf1d6

15. Wu, J., Xia, M., Wang, J. et al.: Effect of electrode induction melting gas atomization on powder quality: satellite formation mechanism and pressure. Materials. 2023; (16), 2499. https://doi.org/10.3390/ma16062499

16. Wang, P., Li, X., Zhou, X. et al.: Numerical simulation on metallic droplet deformation and breakup concerning particle morphology and hollow particle formation during gas atomization. Transactions of Nonferrous Metals Society of China. 2024; (34), 2074–2094. https://doi.org/10.1016/S1003-6326(24)66526-X

17. Ibrahim, M., Gobber, F., Hulme, C. et al.: Influence of atomizing gas pressure on microstructure and properties of nickel silicide intended for additive manufacturing. Metals. 2024; (14), 930. https://doi.org/10.3390/met14080930

18. Mostafaei, A., Hilla, C., Stevens, E. et al.: Comparison of characterization methods for differently atomized nickel-based alloy 625 powders. Powder Technology. 2018; (333), 180–192. https://doi.org/10.1016/j.powtec.2018.04.014

19. Kan, W., Chiu, L., Lim, C. et al.: A critical review on the effects of process-induced porosity on the mechanical properties of alloys fabricated by laser powder bed fusion. Journal of Materials Science. 2022; (57), 9818–9865. https://doi.org/10.1007/s10853-022-06990-7

20. Yodoshi, N., Endo, T., Masahashi, N.: Evaluation of porosity in gas-atomized powder by synchrotron x-ray CT and investigation of the effect of gas species, Materials Transactions. 2021; 10(62), 1549–1555. https://doi.org/10.2320/matertrans.MT-Y2021001

21. Luo, S., Wei, Q., Ouyang, Y. et al.: The impact of co-axial gas technology on the morphology of powder by gas atomisation and the additive manufactured

mechanical performance. Virtual and Physical Prototyping. 2024; (19), e2375107. https://doi.org/10.1080/17452759.2024.2375107

22. Zhang, L., Xu, W., Li, Z. et. al.: Mechanism of rapidly solidified satellites formation in gas atomized powders: Simulation and characterization. Powder Technology. 2023; (418), 118162. https://doi.org/10.1016/j.powtec.2022.118162

23. Brika, S., Letenneur, M., Dion, C. et al.: Influence of particle morphology and size distribution on the powder flowability and laser powder bed fusion manufacturability of Ti-6Al-4V alloy. Additive Manufacturing, 2019; 100929. https://doi.org/10.1016/j.addma.2019.100929

24. Li, H., Zhang, S., Chen, Q. et al.: High-quality spherical silver alloy powder for laser powder bed fusion using plasma rotating electrode process. Micromachines. 2024; (15), 396. https://doi.org/10.3390/mi15030396

25. Liu, Y., Zhao, X., Lai, Y. et al.: A brief introduction to the selective laser melting of Ti6Al4V powders by supreme-speed plasma rotating electrode process. Progress in Natural Science: Materials International. 2020; (30), 94–99. https://doi.org/10.1016/j.pnsc.2019.12.004

26. Zhao, Y., Cui, Y., Numata, H. et al.: Centrifugal granulation behavior in metallic powder fabrication by plasma rotating electrode process. Sci Rep. 2020; (10), 18446. https://doi.org/10.1038/s41598-020-75503-w

27. Cui, Y., Zhao, Y., Numata, H. et al.: Effects of plasma rotating electrode process parameters on the particle size distribution and microstructure of Ti-6Al-4 V alloy powder. Powder Technology. 2020; (376), 363–372. https://doi.org/10.1016/j.powtec.2020.08.027

28. Han, Z., Zhang, P., Lei, L. et al.: Morphology and particle analysis of the Ni_3Al-based spherical powders manufactured by supreme-speed plasma rotating electrode process. Journal of Materials Research and Technology. 2020; (9), 13937–13944. https://doi.org/10.1016/j.jmrt.2020.09.102

29. Wang, Z., Wang, J., Xu, S. et al.: Influence of powder characteristics on microstructure and mechanical properties of Inconel 718 superalloy manufactured by direct energy deposition. Applied Surface Science. 2022; (583), 152545. https://doi.org/10.1016/j.apsusc.2022.152545

30. Zhong, C., Chen, J., Linnenbrink, S. et al.: A comparative study of Inconel 718 formed by high deposition rate laser metal deposition with GA powder and PREP powder. Materials & Design. 2016; (107), 386–392. https://doi.org/10.1016/j.matdes.2016.06.037

31. Korzhyk, V., Kulak, L., Shevchenko, V. et al.: New equipment for production of super hard spherical tungsten carbide and other high-melting compounds using the method of plasma atomization of rotating billet. Materials Science Forum. 2017; (898), 1485–1497. https://doi.org/10.4028/www.scientific.net/msf.898.1485

32. Qiu, J., Yu, D., Qu, Y. et al.: In-flight droplet plasma atomization: A novel method for preparing ultrafine spherical powders. Advanced Powder Technology. 2025; (36), 104757. https://doi.org/10.1016/j.apt.2024.104757

33. Zhang, Q., Yu, D., Liu, F. et al.: Modeling on the size of the pre-breaking molten droplet in plasma atomization for controlling the size of the produced powders. Applied Thermal Engineering. 2023; (232), 121031. https://doi.org/10.1016/j.applthermaleng.2023.121031

34. Kang, I., Park, H., Cho, C. et al.: Development of a plasma and gas hybrid atomization system for the production of metal powder materials. J. Korean Phys. Soc. 2021; (79), 1141–1150. https://doi.org/10.1007/s40042-021-00341-6

35. Kalayda, T., Kirsankin, A., Ivannikov, A. et al.: The plasma atomization process for the Ti-Al-V powder production. J. Phys.: Conf. Ser. 2021; 1942, 012046. https://doi.org/10.1088/1742-6596/1942/1/012046

36. Bobzin, K., Wietheger, W., Burbaum, E. et al.: High-velocity arc spraying of Fe-based metallic glasses with high Si content. J Therm Spray Tech. 2022; (31), 2219–2228. https://doi.org/10.1007/s11666-022-01433-w

37. Yin, Z., Yu, D., Zhang, Q. et al.: Experimental and numerical analysis of a reverse-polarity plasma torch for plasma atomization. Plasma Chem Plasma Process. 2021; (41), 1471–1495. https://doi.org/10.1007/s11090-021-10181-8

38. Korzhik, V. Theoretical analysis of the conditions required for rendering metallic alloys amorphous during gas-thermal spraying. III. Transformations in the amorphous layer during the growth process of the coating. Powder Metall. Met. Ceram. 1992; (31), 943–948. https://doi.org/10.1007/BF00797621

39. Fialko, N., Prokopov, V., Meranova, N. et al.: Thermal physics of gas-thermal coatings formation processes. State of investigations. Fizika i Khimiya Obrabotki Materialov. 1993; (4), 83–93.

40. Jing, H., Yu, Shi, Gang, Zh. et al.: Minimizing defects and controlling the morphology of laser welded aluminum alloys using power modulation-based laser beam oscillation. J. Manufacturing Processes. 2022; (83), 49–59. https://doi.org/10.1016/j.jmapro.2022.08.031

41. Skorokhod, A., Sviridova, I., Korzhik, V.: Structural and mechanical properties of polyethylene terephthalate coatings as affected by mechanical pretreatment of powder in the course of preparation. Mekhanika Kompozitnykh Materialov. 1994; (30), 455–463.

42. Fialko, N., Dinzhos, R., Sherenkovskii, Y. et al.: Influence on the thermophysical properties of nanocomposites of the duration of mixing of components in the polymer melt. Eastern-European Journal of Enterprise Technologies. 2022; (116), 25–30. https://doi.org/10.15587/1729-4061.2022.255830

43. Gu, Y., Zhang, W., Xu, Y. et al.: Stress-assisted corrosion behaviour of Hastelloy N in FLiNaK molten salt environment. npj Mater Degrad. 2022; (6), 90. https://doi.org/10.1038/s41529-022-00300-x

44. Li, X., Cui, L., Shonkwiler, S. et al.: Automatic characterization of spherical metal powders by microscope image analysis: a parallel computing approach. J. Iron Steel Res. 2023; (30), 2293–2300. https://doi.org/10.1007/s42243-022-00907-z

45. Nie, Y., Tang, J., Teng, J. et al.: Particle defects and related properties of metallic powders produced by plasma rotating electrode process (PREP). Adv. Powder Technol. 2020; (31), 2912–2920. https://doi.org/10.1016/j.apt.2020.05.018

46. Skorokhod, A., Sviridova, I., Korzhik, V.: The effect of mechanical pretreatment of polyethylene terephthalate powderon the structural and mechanical properties of coatings made from it. Mechanics of Composite Materials. 1995; (30), 328–334. https://doi.org/10.1007/BF00634755

47. Fialko, N., Dinzhos, R., Sherenkovskii, J.: Establishing patterns in the effect of temperature regime when manufacturing nanocomposites on their heat-conducting properties. Eastern-European Journal of Enterprise Technologies. 2021; 4(5112), 2126. https://doi.org/10.15587/1729-4061.2021.236915

48. Fialko, N., Dinzhos, R., Sherenkovskii, J. et al.: Establishment of regularities of influence on the specific heat capacity and thermal diffusivity of polymer nanocomposites of a complex of defining parameters. Eastern-European Journal of Enterprise Technologies. 2021; (114), 34–39. https://doi.org/10.15587/1729-4061.2021.245274

49. Borisov, Y., Kunitskii, Y., Korzhik, V. et al.: Structure and some physical properties of plasma-sprayed coatings of the nickel boride Ni_3B. Powder Metallurgy Metal Ceramics. 1986; (25), 966–969. https://doi.org/10.1007/BF00797102

50. Fialko, N., Prokopov, V., Sherenkovskii, Y. et al.: Mathematical simulation of 3D temperature fields in the articles during gas thermal sputtering of alloys liable to amorphous transformation. Elektronnaya Obrabotka Materialov. 1992; (5), 20–23.

51. Okuniewski, W., Walczak, M., Szala, M. Effects of shot peening and electropolishing treatment on the properties of additively and conventionally manufactured Ti6Al4V alloy: A review. Materials. 2024; (17), 934. https://doi.org/10.3390/ma17040934

52. Borisov, Y., Korzhyk, V., Revo, S.: Electric and magnetic properties of thermal spray coatings with an amorphous structure / Borisov, Y., Korzhyk, V., Revo, S. Proceedings of the International Thermal Spray Conference. 1998; 687–691. https://doi.org/10.31399/asm.cp.itsc1998p0687

53. Ledwig, P., Pasiowiec, H., Cichocki, K. et al.: Tailoring microstructure and mechanical properties of additively manufactured Inconel 625 by remelting strategy in laser powder bed fusion. Metall Mater Trans A. 2024; (55), 2485–2508. https://doi.org/10.1007/s11661-024-07412-w

54. Zhao, Y., Aoyagi, K., Daino, Y. et al.: Significance of powder feedstock characteristics in defect suppression of additively manufactured Inconel 718. Additive Manufacturing. 2020; (34), 101277. https://doi.org/10.1016/j.addma.2020.101277

55. Moussaoui, K., Rubio, W., Mousseigne, M. et al.: Effects of selective laser melting additive manufacturing parameters of Inconel 718 on porosity, microstructure and mechanical properties. Materials Science and Engineering: A. 2018; (735), 182–190. https://doi.org/10.1016/j.msea.2018.08.037

56. Gao, S., Kryvtsun, I., Korzhyk, V. et al.: Features of the process of formation and dispersion of a liquid layer and formation of powder particles in plasma-arc atomization of current-conducting solid and flux-cored wires. Advances in Science and Technology Research Journal. 2025; (19), 58–72. https://doi.org/10.12913/22998624/201362